Synergy between microstructure anisotropy and size effects on the ductile failure of Hastelloy X printed by Laser Power Bed Fusion

Benoit Vieille, Ronan Henry, L. Avegnon, M.P. Sealy, Q. Sirvin, D. Texier, C. Keller

Synergy between microstructure anisotropy and size effects on the ductile failure of hastelloy X printed by laser power bed fusion

B. Vieille [a,*], R. Henry [a], L. Avegnon [a], M.P. Sealy [b], Q. Sirvin [c], D. Texier [c], C. Keller [d]

[a] Normandie Univ, UNIROUEN, INSA Rouen, CNRS, Groupe de Physique des Matériaux, 76800, Saint-Étienne-du-Rouvray, France
[b] Purdue University, School of Mechanical Engineering, 610 Purdue Mall, West Lafayette, IN, 47907, USA
[c] Institut Clément Ader (UMR CNRS 5312), Université de Toulouse, ISAE-SUPAERO – UPS – IMT Mines Albi – INSA, 10 Av. E. Belin Cedex 4, F-31055, Toulouse, France
[d] Laboratoire Génie de Production, Université de Technologie de Tarbes Occitanie Pyrénées, Université de Toulouse, 47 Av. d'Azereix, 65000 Tarbes, France

This work addresses the effect of the microstructural anisotropy, both morphological and crystallographic due to fabrication strategy, and the size-effects on the fracture behavior of Hastelloy X superalloys printed by Laser Power Bed Fusion (LPBF-HX). It aims at specifically investigating the role played by crack orientation (perpendicular or co-linear to sample lasing planes) on the fracture toughness values of LPBF-HX. Micro-canti-lever bending tests have been conducted on vertically or horizontally built specimens to estimate the fracture toughness at the microscopic scale depending on the initial notch orientation. LPBF-HX results in complex microstructural features at the micro- and mesoscale, which significantly impair the fracture mechanisms. At both microscopic and macroscopic scales, cracking occurs along with a ductile tearing. A simple analytical model has been applied to account for the size effect on the fracture behavior depending on the building direction and notch orientation. This model provides internal characteristic lengths, d_0, which is a key parameter for transition rules from small to large scale. In horizontal specimens, the value of d_0 is equal to 1.33 mm, whereas it slightly increases to 1.57 mm in vertical specimens. The knowledge of the size effect law using internal characteristic lengths is crucial for the determination of the R-curve at different scales.

Fracture toughness, Additive manufacturing, Ductile failure, Microstructure, Micromechanical testing

1. Introduction

Additive Manufacturing (AM) and in particular Laser Powder Bed Fusion, has opened new design possibilities by enabling the fabrication of complex, topology-optimized components. Such optimization often leads to the presence of thin or intricate geometries, making it essential to assess the mechanical performance of materials independently of the dimension of the part, i.e., thin walls or bulk parts. Moreover, the LPBF process generates a complex hierarchical microstructure—characterized by rapid solidification, fine cellular substructures, melt pool boundaries, and residual porosity —which can significantly influence key mechani-cal properties. Regarding monotonic mechanicals properties, their dependence to those microstructure elements have been addressed in literature. For instance, it has been reported that cellular substructures are responsible for almost half the large yield stress of Ni20Cr LPBF alloys [1,2]. Those substructures seem also to play an important role on the wear resistance [3]. Nevertheless, the influence of these microstructural length scale of LPBF material on the fracture toughness remains widely unexplored as well as the influence of the specimen size, and more specifically when their fracture behavior is characterized by ductile tearing. To answer this question, it is necessary to explore the fracture mechanisms at the micro and macro scales.

Indeed, from a fracture mechanics perspective, the crack growth resistance of micro- and sub-micrometer-sized samples is of prime importance, emphasizing challenges and adaptations required due to size reduction in many industrial applications [6]. For most of the ductile materials, fracture mechanics tests on micro-sized samples exhibit a size dependence in fracture resistance. According to tests standards at macroscale, it is crucial to use specimens large and wide enough to achieve plane strain conditions and minimize the influence of these size effects and local plasticity for accurate fracture toughness measurements at macroscopic scale [7]. The major reason for the size dependency of fracture toughness is the existence of a Fracture Process Zone around the crack tip. If the FPZ is large compared to the specimen size, the fracture toughness becomes more dependent on the specimen

Glossary

AM	Additive manufacturing
FIB	Focused Ion Beam
LEFM	Linear Elastic Fracture Mechanics
LPBF	Laser Powder Bed Fusion
EDM	Electrical Discharge Machining
FCC	Face-Centered Cubic
FPZ	Fracture Process Zone
SEM	Scanning Electron Microscope
SENB	Single Edge Notched Bending

size [8]. When it comes to ductile fracture, the size-dependence of fracture toughness is more complex to establish since several factors can concomitantly coexist, including the microstructure, the grain size, the plasticity at the crack tip, and environmental factors such as elevated temperatures [9]. Furthermore, an increase in the "grain size-to-specimen size" ratio leads to higher variability in fracture toughness values due to microstructural heterogeneity [10]. For small specimens whose fracture behavior is plasticity-dominated, the fracture toughness J_{Ic} often exhibits size dependence due to the ratio of "crack length-to-specimen size", the stress concentration effects and the finite size of the FPZ. The size effect on apparent fracture toughness $J_{Ic,app}$ is therefore determined from the fracture toughness value of "macroscopic" specimens J_{Ic} and a function that accounts for geometric factors and plastic zone size [11]:

$$J_{Ic,app} = J_{Ic}. \quad (1)$$

This accounts for the transition from plane strain (low toughness) to plane stress (higher toughness) as specimen size decreases. The knowledge of the size effect on the fracture behavior is utmost important to determine the R-curve, describing how the energy resistance to crack growth depends on the crack length [12]. Measuring the local crack propagation behavior in a quantitative manner has always been a challenge in the field of fracture mechanics [9]. In-situ micro-cantilever testing inside a Scanning Electron Microscope is a promising technique for such investigations thereof. However, quantitative fracture mechanics using such microsized experiments is fairly challenging. Brinckman et al. gave guidelines for micro-cantilever design and quantification of the changes in fracture toughness, if the conventional fracture test standards cannot be fulfilled [13]. Miniaturized fracture beam experiments offer the ability to identify the fracture toughness at the microstructure phase and more specifically, the one of single phase and particular grain boundaries cases. Conversely, large-scale experiments only reveal homogenized material properties. Wang et al. have conducted experiments of fracture toughness with non-standard SENB specimens to investigate size effects on the ductile fracture of steel for different thicknesses [14]. The ductile fracture toughness increases firstly with increased size of the plastic deformation zone and plastic fracture strain under general yielding conditions [15].

In semi-brittle materials, LEFM is inapplicable due to the large plastic zone in relation to the micrometer sample size, and elastic-plastic fracture mechanics has to be applied [16,17]. For materials exhibiting ductile failure, the question remains relatively open although the literature suggests the validity of the J-integral as a small-scale failure criterion [18,19]. By performing three-point bending tests on nickel-based superalloys at micro (in the order of 100–200 μm) and macroscopic (in the order of several tens of mm) scales, toughness values were evaluated by various calculation methods, including techniques derived from the J-integral (ASTM E1820). The main result of this work is that the critical toughness values at the macroscale are two orders of magnitude higher (155 kJ/m^2 at the macroscale vs 1.3 kJ/m^2 at the microscale).

At the macroscopic scale, the influence of microstructure anisotropy and the original crack orientation (perpendicular or parallel to the lasing planes) on the ductile fracture behavior of Hastelloy X printed by Laser Powder Bed Fusion (LPBF), has been recently investigated [20,21]. Due to the material characteristics inherited from the LPBF process, the highest fracture toughness value (about 1360 kJ/m^2) was obtained in vertically built specimens (V) with an original crack parallel to the lasing plane whereas horizontally built specimens (H) with the second crack orientation exhibited value of about 1042 kJ/m^2 [21]. A non-self-similar cracking is specific to V specimens revealing a more tortuous crack path than in H specimens with self-similar cracking (the crack propagates along the initial plane of the notch). In both cases, ductile failure is driven by both transgranular and intergranular modes. In metals processed by AM techniques, this is attributed to their often-metastable microstructures, their layer-by-layer mesostructures, and their anisotropic failure characteristics that lead to pronounced variability in the fracture toughness data for materials with similar ductility [22].

In this context, the question of microstructure anisotropy on the fracture toughness of metals processed by AM methods is still unanswered when it comes to small-scale testing. The evaluation of the microscale toughness is classically based on isotropic 2D models although the majority of AM materials are mechanically anisotropic. To better understand the possible size-effect in hastelloy X printed by LPBF, the analytical model initially proposed by Bazant was adapted to ductile failure [11]. The present study intends to document size effects from the macro-to the microscale on the fracture toughness behavior of the HX-LPBF having anisotropic mechanical responses inherent to the fabrication process.

2. Materials and experimental set-up

2.1. Materials and specimens

2.1.1. Materials

This investigation was performed on a Hastelloy X Ni-based superalloy obtained by additive manufacturing. The precursor powder of this material was provided by Auber and Duval with powder particle average diameter of about 30 μm. The chemical composition of this alloy following standards is reported in Table 1. The fabrication of the Hastelloy X materials was performed on a SLS EOS M400-4 laser powder bed fusion (LPBF) machine at Volum-E company (France).

The fabrication process parameters used for the manufacturing are summarized in Table 2. Different sampling directions were investigated in the present study to document the anisotropic mechanical response of the material (see Fig. 1) at different scales. All samples are investigated as-built, without any post manufacturing heat-treatment. Preliminary mechanical characterizations were performed using tensile tests and three points bending using SENB specimens (in agreement with ASTM E1820 test standard) on the alloy in different fabrication directions and properties are summarized in Table 3 [21,23]. Elastic properties, yield stress, ultimate tensile strength, fracture toughness and Irwin plastic zone radius values were determined in both horizontal and vertical configurations.

2.1.2. Specimen fabrication and preparation

Parallelepipedic specimens were manufactured by LPBF according to two building directions, H and V (Horizontal and Vertical, respectively – Fig. 1). Investigating the fracture behavior at different scales needs the manufacturing of macro, meso and micro-cantilever bending tests. Due to the inherent constraints of in-situ bending test in a Scanning Electron

Table 1
– Hastelloy X (LPBF) specimens: standard chemical composition of powder (% wt.).

Ni	C	Si	Mn	P	S	Co	Mo	W	Cr	Fe
Base	0.15	1	1	0.04	0.03	2.5	10	1	23	20

Table 2
– Laser Power Bed Fusion manufacturing parameters (SLM EOS M400-4).

Laser power (W)	Laser scanning speed (mm/s)	Hatch distance (mm)	Powder layer thickness (µm)	Layer to layer angle misorientation (°)
288	960	0.11	40 µm	67

Microscope, comparatively to previous investigations on fracture toughness [21], fixed-end simple bending has to be considered here for both macro and micro tests. For each scale, two crack orientations with respect to the lasing planes were considered: one with the crack perpendicular to the lasing plane, called Horizontal and illustrated in Fig. 1b and a second one, with the crack lying in a lasing plane, called Vertical and illustrated in Fig. 1c. The macro-cantilever bending specimens were machined by EDM with dimensions of about 15x3x4.9 mm (l x b x d, see Fig. 1).

The initial crack, in this macro configuration, is about 1.5 mm deep. The micro-cantilever specimens were prepared with a plasma Focus Ion Beam (Helios5 PFIB CXe, ThermoFisher Scientific) with a SENB geometry and rectangular cross-section (Fig. 2). The approximate dimensions of the cantilever (l x b x d) were: 100 × 20 × 20 µm^3. The initial notch, obtained using plasma FIB-machining, was approximately of $a_0 = 8$ µm deep. A first step, using a low current directly on the surface and edge of the sample, aims to position the notch (notch depth parallel to the FIB direction). Next, a high current is used to create the preform geometry of the beam, followed by a 90° machining step to remove the material beneath the future beam. Each beam surface was then machined with progressively lower currents to make the surfaces straighter, smoother and to reduce damage induced by FIB. It is worth noticing that an intermediate scale with submillimeter dimensions was not targeted as both EBM or FIB are not suitable to manufacture accurate samples in this dimension range (see Fig. 3).

Considering the potential impacts of FIB-induced effects, it is expected that gallium implantation and surface amorphization may affect a thin layer of about a few tens of nanometers which are expected negligible compared to the 20 µm width of the micro sized samples [5, 24].

2.2. Experimental methods

2.2.1. Flexural testing at macroscopic scale

The flexural tests were conducted on macro-cantilever specimens using a hydraulic testing machine MTS 810 equipped with a 100 kN load cell. The tests were performed at room temperature in displacement-controlled mode at a displacement rate of 2 mm min^{-1}. From the load (F) - displacement (δ) data, the maximum bending stress σ_{max} and strain ε_{max} are computed at the fixed end ($y = 0$ and $z = d/2$) as follows:

$$\sigma_{max} = \frac{6FL}{bd^2} \text{ and } \varepsilon_{max} = \frac{6FL}{Ebd^2} \quad (2)$$

where L is the distance from the load application point to the embedded extremity of the cantilever beam, b and d are the width and thickness of the beam, respectively. E is the Young's modulus.

The repeatability of the results was ensured by considering at least five specimens in every configuration. A high-speed monochromic Grasshopper® camera with a 2.3MPix resolution was used to perform in-situ monitoring of the crack propagation at the surface. The acquisition frequency was set to 20Hz.

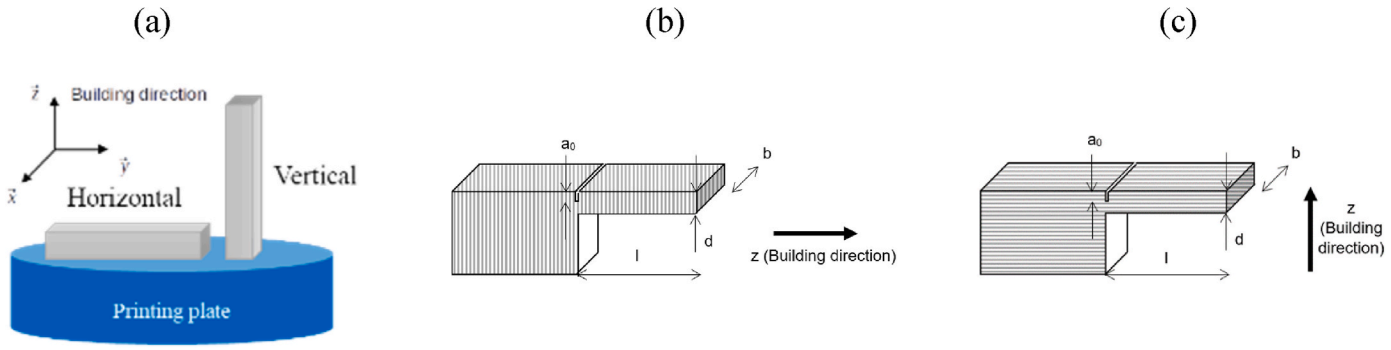

Fig. 1. – Geometrical configuration of the investigated HX specimens manufactured by LPBF: (a) parallelepipedic parts – (b) and (c) illustration of the sample geometry for both micro and macro configuration (dimensions are given in the text) with the two cracks orientation configuration, namely vertical and horizontal.

Table 3
– *Mechanical properties in tension of LPBF HX specimens in horizontal and vertical built configurations from previous studies* [21,23].

	Young's modulus (GPa)	Poisson ratio	Yield strength (MPa)	Ultimate tensile stress (MPa)	J_{Ic} (kJ/m^2)	r_p (µm)
Horizontal built	220	0.29	649	697	1042 ± 165	41
Vertical built	220	0.29	609	785	1360 ± 144	47

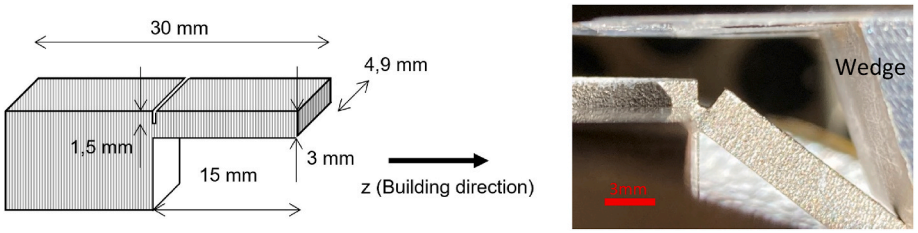

Fig. 2. – Notched macro-cantilever testing of HX LPBF specimens at macroscopic scale: (a) specimen dimensions - (b) observation of the cantilever specimen subjected to a flexural load applied by a wedge.

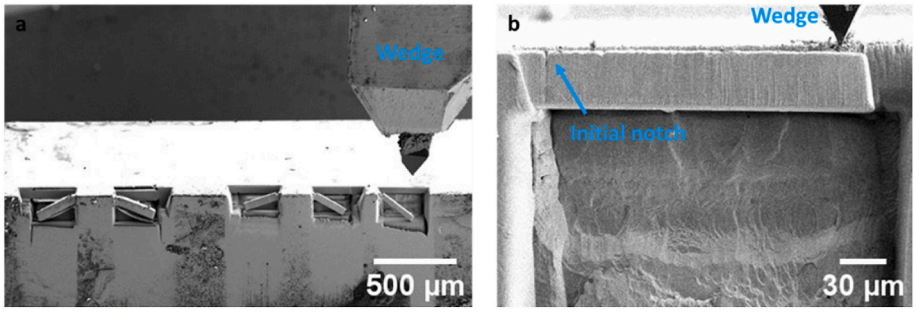

Fig. 3. – Notched micro-cantilever testing of HX LPBF specimens at microscopic scale: (a) FIB machining and location of the micro-cantilever specimens – (b) observation of the micro-cantilever specimen subjected to a flexural load applied by a wedge.

2.2.2. Flexural testing at microscopic scale

The micro-cantilever specimens were mechanically loaded using an *in-situ* nano-indenter (PI87R, Brucker) equipped with a wedge tip inside a Zeiss XB540 scanning electron microscope. The specimens are loaded in displacement-controlled mode at a displacement rate corresponding to a strain rate of approximately 5.10^{-4} s^{-1}. In order to monitor the crack growth, the micro-cantilever was placed in front of the SEM column during mechanical loading to get a sequence of images at different times of the loading. Crack growth was directly evaluated during ***in-situ* experiments by means of SEM images acquisition.** Three specimens were tested in each configuration.

The J-integral estimation procedure, as recommended by the ASTM E1820 test standard, requires adaptations for microscale testing [25]. More precisely, the compliance calibration was not explicitly performed due to the challenges of micro-cantilever geometry, but boundary conditions (e.g., wedge loading) were accounted for via SEM monitoring. Potential error margins (e.g., from load-displacement measurements) and their impact on fracture toughness values may stem from the difficulty to ensure the reproducibility of boundary conditions as well as the accurate machining of the notch. Indeed, possible causes for errors include notch positioning variability (e.g., within grains vs. at grain boundaries), microstructural heterogeneity (e.g., varying grain orientations), or localized defects like porosity. These factors may disproportionately affect horizontal specimens due to their layer-wise microstructure. To enhance robustness, sample sizes should be increased and the control of a precise notch placement should be improved.

2.2.3. Fracture toughness computation and J-R curves

Force and displacement were recorded during mechanical loading at both macro- and microscales. Stable crack growth was observed for all cantilevers and R-curves representing the fracture energy J_I vs. crack growth Δa were obtained. The procedure for obtaining the *J-R* curves is described in ASTM E1820-01 standard test method [25]. In materials with ductile fracture behaviors, the mode I fracture toughness J_I is computed from the elastic-plastic fracture mechanics concepts defined as follows:

$$J_I = J_{elastic} + J_{plastic} \tag{3}$$

with $J_{elastic}$ computed from the mode I critical stress intensity factor K_{Ic} and the engineering constants of the materials in orthotropic materials [26,27]:

$$J_{elastic} = C_I.K_{Ic}^2 \tag{4}$$

with $C_I = \sqrt{\frac{1}{2E_xE_y}}\sqrt{\sqrt{\frac{E_x}{E_y}} - \nu_{xy} + \frac{E_x}{2G_{xy}}}$ in plane-stress conditions.

The plastic component $J_{plastic}$ is obtained from the mechanical energy dissipated A_{pl} corresponding to the area under the force-displacement curve:

$$J_{plastic(i)} = \left[J_{plastic(i-1)} + \frac{\eta_{pl(i-1)}}{b_{(i-1)}}\left(\frac{A_{pl(i)} - A_{pl(i-1)}}{B_N}\right)\right].\left[1 - \gamma_{pl(i-1)}\left(\frac{a_{(i)} - a_{(i-1)}}{b_{(i-1)}}\right)\right] \tag{5}$$

where $\eta_{pl(i-1)} = 1.9$ and $\gamma_{pl(i-1)} = 0.9$ are plastic factors in agreement with ASTM E1820 standard test method in the case of SENB specimens loaded in bending. B_N is the net specimen thickness. $a_{(i)}$ and $b_{(i)} = w - a_{(i)}$ are the crack length and the unbroken ligament at iteration (i), respectively. These values are computed for each iteration (i).

The tearing modulus T was also calculated to get a better understanding of the resistance to crack propagation [28]:

$$T = \frac{E}{\sigma_y{}^2}\frac{dJ}{da} \tag{6}$$

where E is the Young Modulus and σ_y is the yield stress determined from monotonous tensile tests [23].

According to ASTM E1820 standard, the Irwin's requirement should be met to validate the value of fracture toughness [25]. It stipulates that the size of the plastic zone depends on the applied stress, the mechanical properties of the material and the size of the crack. The higher the applied stress, the larger the plastic zone and the more likely the crack will propagate. In addition, crack propagation occurs when the elastic strain energy stored in the material is equal to the energy required to create a new crack surface. This occurs when the size of the plastic zone reaches a critical size called the critical crack length r_p. The size of this plastic zone r_p around the crack tip in the case of mode I loading and plane-strain state can be calculated as follows:

$$r_p = \frac{1}{3\pi}\left(\frac{K_{Ic}}{\sigma_y}\right)^2 \tag{7}$$

2.2.4. Size-effect analytical model

In ductile metals, the crack propagation is blunted by a zone of local yielding [29]. As aforementioned, this blunting causes deviations from the structural size effect known from LEFM. If the size of the FPZ – resulting from local plasticity - encompasses all or most of the specimen or structure volume, the failure is determined by a plastic criterion [29]. To separate the size effect from other factors, structures of different sizes but geometrically similar shapes must be considered (e.g., beams with the same crack length-to-depth – c/d – ratio). Bazant et al. have addressed the question of size effect for elastic-plastic fracture of metals. σ_N represents the nominal stress at failure characterizing the stress state at a certain critical load P of the structure. If one considers the plot of $log\ (\sigma_N)$ versus $log\ (\lambda)$ where $\lambda = \frac{d}{d_0}$ dimensional size parameter and d_0 an internal characteristic length, the locus of all failure states according to any kind of strength criterion is a horizontal line regardless of whether the material has an elastic, plastic or viscoplastic behavior. In elastic-plastic fracture, the crack tip is blunted by yielding, and the size of this zone develops ahead of the crack tip [31]. Local plasticity

depends on the triaxial stress state. Small scale testing results in a plane-stress state and low triaxiality ratios, ultimately causing larger plastic deformations near the crack tip. In ductile materials, the size effect law defines the nominal stress at failure from the characteristic dimension of the structure d as follows [29,30]:

$$\sigma_N = \frac{B\sigma_y}{\sqrt{1+\frac{d}{d_0}}} \tag{8}$$

where B is a constant. The values of B and d_0 depend on the geometry of the structure

The transition from small to large scale being of interest for many practical applications, it requires the internal characteristic length d_0 to be determined. In addition, the knowledge of the size effect law is crucial for being able to determine the R-curve without having to measure the crack growth [32]. According to Nguyen et al., the R-curve representing the fracture energy as a function of the crack length can be defined as follows [33]:

$$R(c) = J_f\left[1+\frac{k_0}{c+k_1.c^n}\right]^{-m} \tag{9}$$

where J_f represents the fracture energy corresponding to the final asymptotic value of R (assuming the complete failure of the structure). A linear regression is considered to fit the values of k_1, m, n to the experimental data points using least square error minimization [29]. Indeed, equation (9) can be transformed to the form $Y' = A'.X' + C'$, in which:

$$Y' = ;\ X' = c^{n-1};\ A' = k_1/k_0 \text{ and } C' = 1/k_0 \tag{10}$$

2.2.5. Microstructure analysis

In order to correlate the fracture toughness analysis to the material microstructure, grain orientation maps were acquired using a JEOL 7900 F Scanning Electron Microscopy (SEM) coupled with Electron BackScattered Diffraction (EBSD) (Hikari camera, EDAX). To this aim, undeformed macroscopic samples manufactured vertically and horizontally were prepared using conventional metallographic techniques followed by electropolishing (A2 Struers Electrolyte, 20V, 40s). EBSD maps of 1 × 1 mm^2 were obtained at 20 kV on the sample surface perpendicular to the notch plane (i.e., the plane in contact with the punch) and cleaned with standard procedure (grain dilatation using a grain size threshold of four time the step size).

3. Results and discussion

3.1. Macro-vs. micro-cantilever fracture behavior

Considering the definitions of bending stress and strain given in equation (2), the bending behaviors at both macro and micro-scales can be compared (Fig. 4). These definitions of bending stress and strain are helpful to normalize the load and displacement data with respect to specimens' dimension to ease the comparison. Different features may be appreciated from these curves including the yield strength value, the strain at failure and ultimate strength. Compared to macroscale values, it clearly appears that the elastic limit is much higher (about 900 MPa vs 300 MPa) in microscale specimens (smaller is stronger effect) as is already well documented in literature [4,6]. This conclusion is similar regardless the building direction (H or V). At macroscale, no significant differences were found between the two configurations (H or V) in terms of overall bending behavior, except a slight increase in the bending strain at failure. At microscale, necking is more pronounced in the V configuration, suggesting that local plastic deformation develop more easily when the lasing planes are parallel to the initial notch, *i.e.*, when the stress concentration (associated with an opening mode) contributes to split the lasing planes from one another. As a result, the strain hardening is different and it is expected to reflect on the fracture toughness values at initiation and the tearing modulus. To conclude, the bending curves clearly emphasize there is a strong size-dependence in HX printed by LPBF. The question is now to try understand the underlying reasons for these differences.

By conducting bending tests on notched cantilevers at both macro- and microscales, a **comprehensive understanding** of how materials behave (elastic, plastic but also fracture behaviors) under bending loads across different length scales is gained, improving **design reliability, material selection, and failure prediction models (**section 2.2.4**)**. In addition, the specific study on the influence of lasing planes orientation with respect to the initial notch (Fig. 1) is valuable to determine the role played by anisotropic (distribution and shape of grains) and composite effects (the layer wise architecture of LPBF specimens) on the initiation and the propagation of cracks [21]. Macroscale testing classically provides valuable design values in agreement with standard test method for measurement of fracture toughness [25]. References values are obtained from these tests provided the specimen's dimensions requirements are met to foster plane-strain conditions. These requirements are usually not fulfilled at microscale. Microscale testing allows the size effects on mechanical properties to be investigated, with a focus on how material properties like elasticity, strength and toughness change as dimensions shrink. Small-scale tests also provide information on the influence of microstructure features (grain size, grain shape, crystal orientation, and

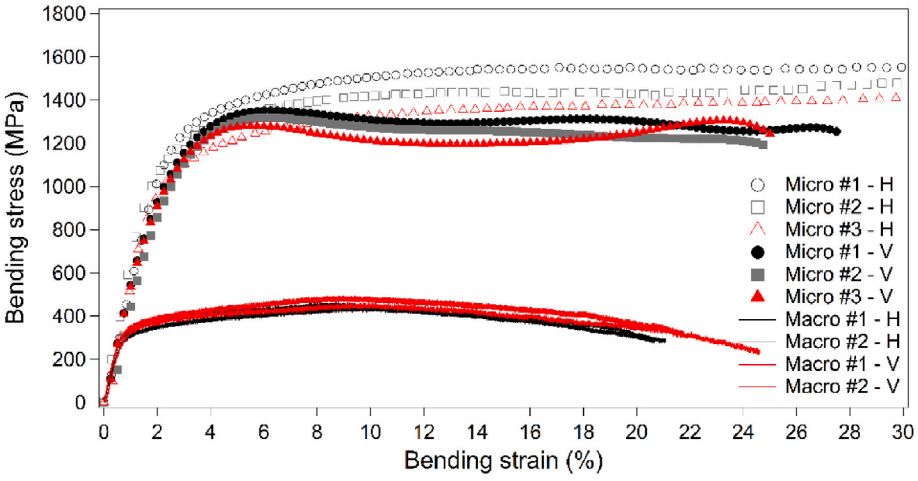

Fig. 4. – Bending responses of macro and micro-cantilevers with a single edge notch: influence of the building direction and testing scale.

defects – dislocations or voids) affect the deformation and failure mechanisms. It also helps to understand if materials behave differently at small scales, often showing increased strength due to constrained dislocation motion (smaller is stronger effect). Finally, the strain gradient effects can be specifically addressed by revealing how strain localization near notches influences failure mechanisms at micro scales.

From the monitoring of SEM images, it is also possible to observe the different stages of specimen's deformation and failure mechanisms during mechanical loading along with the load-displacement curve (Fig. 5). The first stage (Fig. 5a) might be seen as a reference state, highlighting the length of the initial notch, therefore allowing the crack extension to be emphasized. The second stage (Fig. 5b) shows the elastic opening of the notch up to the elastic limit as the mechanical response enters the plastic regime. The next stage (Fig. 5c) corresponds to the blunting of the notch tip associated with the local plastic deformation taking place at the surface of the specimen (plane-stress conditions). Once the crack is initiated, it extends at constant load following a ductile failure mode associated with the highly ductile behavior of HX specimens (Fig. 5d and e). The load-displacement curve suggests that there is no strain hardening and that the mechanical energy brought to the specimens is primarily dissipated by its ductile tearing.

3.2. *J-R curves and fracture toughness estimation*

Based on equations (3)–(5), the fracture toughness values J are computed from the load-displacement data obtained for both testing configurations (horizontal and vertical built). The monitoring of the crack extension Δa by means of the technique introduced on section 2.2.2 (SEM images analysis). It is therefore possible to draw the so-called R-curves (Resistance curve). Fracture testing conducted on notched cantilevers at macroscale did not allow the crack extension to be measured as the crack does not propagate due to extensive plastic deformation occurring at the crack tip (Fig. 2b). As a result, the corresponding R-curves were not obtained in this case. To evaluate the influence of the testing scale on the fracture toughness values, the results obtained at the microscale on notched cantilevers were compared to the ones obtained at the macroscale on SENB specimens [21,23]. It is expected that the effect of the boundary conditions is not significant [34].

At the micro scale, in the J vs Δa curve (cf. Fig. 6), the stable crack propagation is represented by the tearing regime and the tearing modulus – which is usually size-dependent [35] – is computed from the slope of the curve. As recommended by the ASTM standard E1820 in the case of macroscale samples, specimen size-independent fracture toughness values J_0 or $J_{0.2}$ are evaluated by fitting a linear or power law curve to the physical crack extension (excluding blunting) within the 0.15–1.5 mm range. The intersection of this fit with the blunting line or its 0.2 mm offset determines the fracture toughness at initiation. Alfreider et al. also provided a guideline to transfer this concept to micro-samples to determine fracture toughness values J_i or $J_{2\%}$ by intersecting the blunting line or a 2 % offset with a linear fit of the tearing regime [9]. The same approach was considered here to determine the critical fracture toughness in opening mode in both configurations (horizontal and vertical), and the corresponding values are reported in Table 4. Based on equation (6), the tearing modulus values have been also calculated from the date of each test (Table 4).

In AM metals, specific features such as microstructural anisotropy and porosity differentiate LPBF-HX from conventional (wrought or cast) HX, emphasizing the role of build direction and layer-wise fabrication in fracture behavior. Compared to the values obtained in cast specimens (with a Compact Tension geometry) with a similar approach, the fracture toughness of LPBF specimens is virtually 6 times higher [36]. Nevertheless, this improved fracture toughness for AM samples may be related to the original microstructure of the cast samples, which is unknown, and no accurate comparison of the fracture mechanisms is possible. However, the understanding of fracture behavior of HX elaborated by LPBF still needs further investigation.

3.3. *Influence of the initial notch position with respect to the building direction*

First of all, a large fracture toughness difference is observed between the macro and the micro scales, values for the lower scales being three

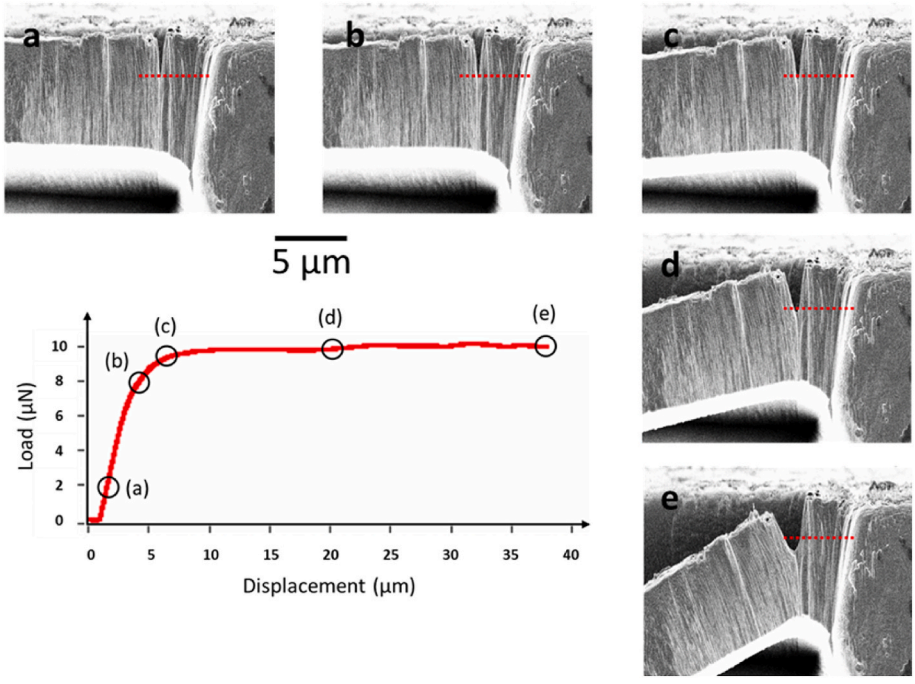

Fig. 5. – In-situ SEM observations of micro-cantilever HX specimens (vertical configuration) subjected to a bending loading: (a) onset of loading – (b) elastic opening of the notch – (c) onset of notch blunting – (d) crack extension – (e) ductile tearing (the red dotted line indicates the length of the initial notch to emphasize further crack extension). (For interpretation of the references to colour in this figure legend, the reader is referred to the Web version of this article.)

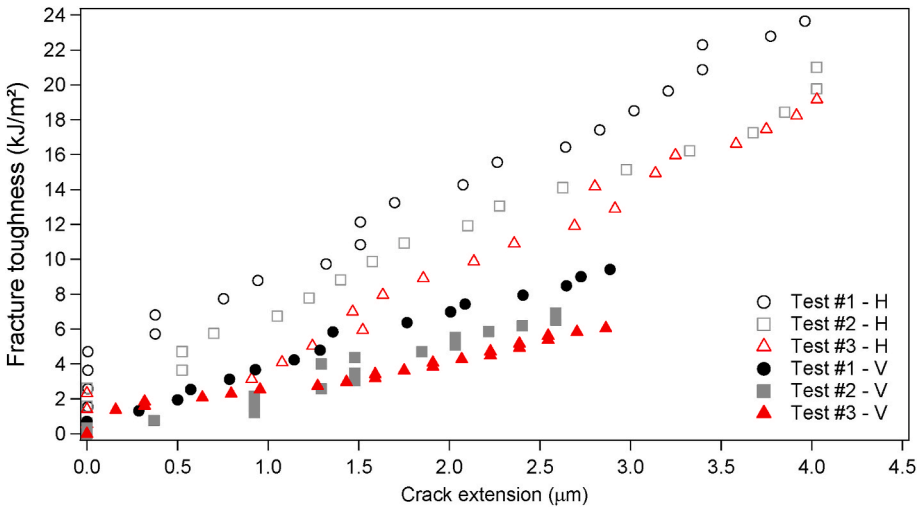

Fig. 6. – Comparison of R-curves of Hastelloy X micro-cantilevers printed by LPBF in horizontal and vertical test configurations.

Table 4
– Microscale testing: influence of building direction on the critical fracture toughness and tearing modulus values for Hastelloy X (LPBF). For each parameter, all measured values are provided alongside an average value followed by the associated standard deviation.

	J_{Ic} (kJ/m^2)	Tearing modulus (–)
Horizontal built	4.66–3.65 – 3.14 average value 4.17 ± 1.37	4.35–4.37 – 4.69 average value 4.47 ± 0.19
Vertical built	1.32–1.22 – 1.37 average value 1.31 ± 0.08	2.61–1.77 – 1.70 average value 2.03 ± 0.51

orders of magnitude lower than the larger one reported in Table 3. Second of all, at microscopic scale, it appears that horizontally built specimens are characterized by higher values of fracture toughness at initiation and tearing modulus than vertically built specimens. This conclusion is opposed to the one obtained on LPBF HX at macroscopic scale (Table 3). Besides, the experimental scattering for the horizontal configuration is significatively larger than the vertical one.

To understand those differences between macro and micro results, Fig. 7a and Fig. b illustrates the initial microstructure for the horizontal and vertical configurations, respectively. In this figure, the grain orientation maps were acquired on the top surface of the samples (surface in contact with the punch), perpendicularly to the crack plane. In these images are also highlighted the four times magnified geometry of the micro samples to illustrate the potential interaction between the microstructure and cracks. The inverse pole figures associated with the horizontal and vertical grain orientation maps are depicted in Fig. 7c and Fig. d, respectively.

On the one hand, Fig. 7a and b shows the typical grain structure resulting from LPBF with a 67° layer-to-layer misorientation for both building directions. Regarding the crystallographic texture (Fig. 7c and d), clear differences arise between the two configurations, with the vertical one exhibiting a stronger texture intensity and distinct crystal orientations aligned with the macroscopic sample axis. Specifically, along the building direction—corresponding to [001] direction in the horizontal configuration and [010] in the vertical one—different poles are observed. In the horizontal case, a {011} plane is aligned with the building direction, whereas in the vertical configuration, a {001} pole dominates. This observation suggests a change in the orientation of the maximal thermal gradient: predominantly vertical and well-defined in the vertical configuration, but more diffuse and inclined at about 45° to the building direction in the horizontal configuration. Such differences in thermal gradient orientation, combined with the resulting microstructural alignment in the microsample, may strongly influence the crack–microstructure interaction and, consequently, the measured fracture toughness values.

Due to the stronger thermal gradient in the vertical configuration, a more pronounced morphological grain texture is expected compared to the horizontal case, with grains elongated preferentially along the building direction. In addition, in the vertical configuration, the microsized specimens are aligned with the building direction. Consequently, the probability of machining a microsample containing only a single grain beneath the crack plane is higher in the vertical than in the horizontal configuration. Second, even when a single grain is located beneath the crack and its orientation relative to the sample plane appears similar, the solidification direction differs between the two configurations. For fcc alloys, dendritic growth follows both the maximum thermal gradient and the {001} crystallographic direction, which are not aligned in the same way for the two manufacturing orientations. Fig. 8 summarizes the dominant crystal orientations (derived from the inverse pole figures in Fig. 7) within the sample plane. In this figure, the crack, the building direction, and the maximum thermal gradient direction are indicated, together with the main crystallographic directions. Dendrites aligned with the {001} directions are also schematically illustrated.

Due to the difference of maximal thermal gradient direction in LPBF and the sample machining direction, dendrites axis is perpendicular to the sample plane in the horizontal direction (oriented either alongside the [100] or [010] direction) whereas their axis lies on the sample plane for the vertical configuration one. In addition, in both cases, the [001] direction associated with these two dominant crystal orientations are aligned with the sample axis which corresponds to the tension-compression direction within the specimen cross section under bending.

These features may explain the trend observed in Table 4 related to the fracture toughness of horizontal and vertical microsized samples. On the one hand, the stronger crystallographic texture associated with the elongated grains in the sample direction for the vertical configuration increases the probability to have similar crystal orientation in different samples as well as reduce the possibility to have an interaction of the crack with a grain boundary. Consequently, the behavior variability

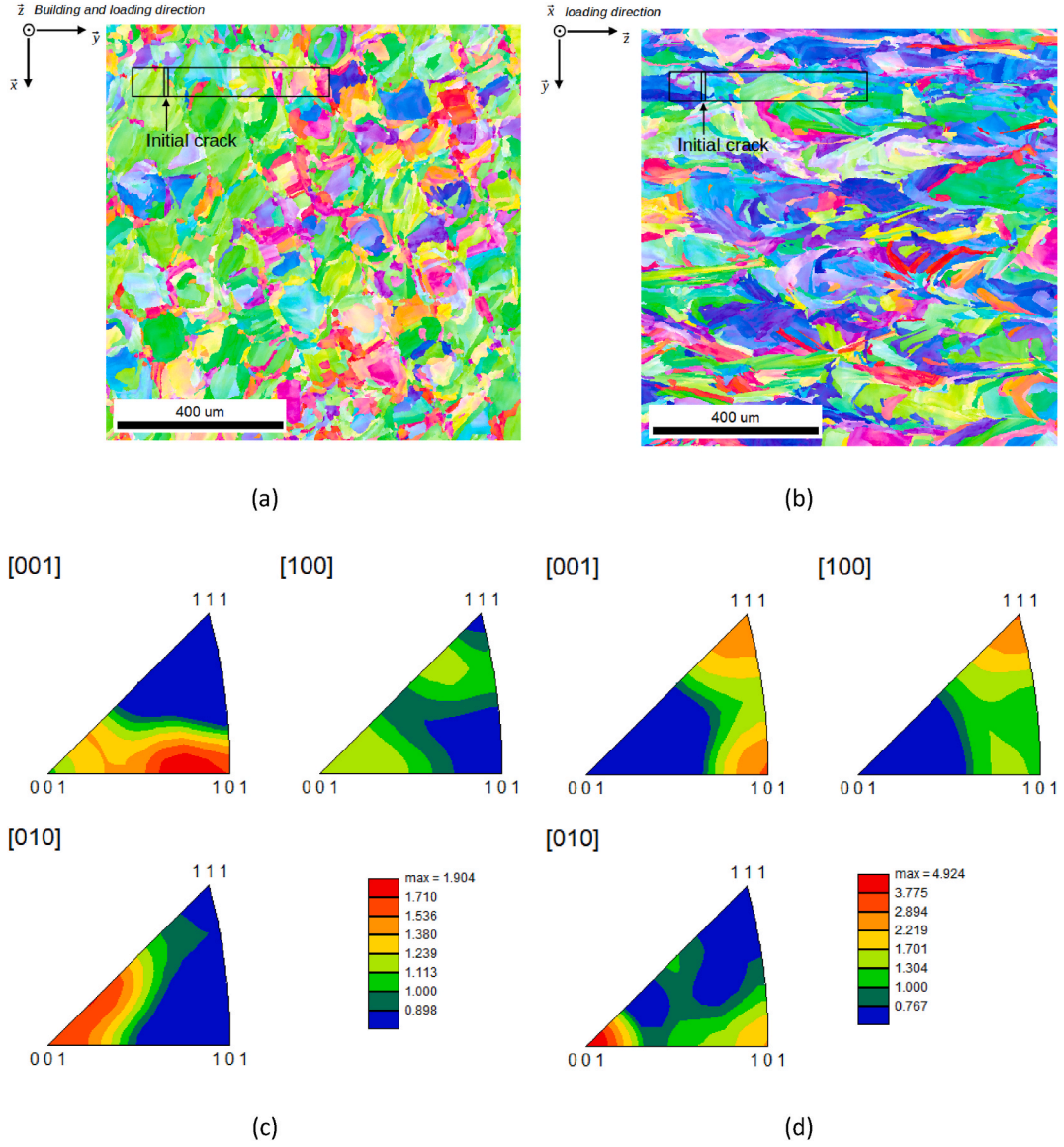

Fig. 7. – Grain orientation maps acquired by EBSD for: (a) the horizontal and (b) the vertical configurations as well as the associated inverse pole figures with (c) horizontal and (d) vertical configurations. For the IPF, [100], [010] and [001] correspond to the vertical, horizontal and normal directions of the grain orientation maps.

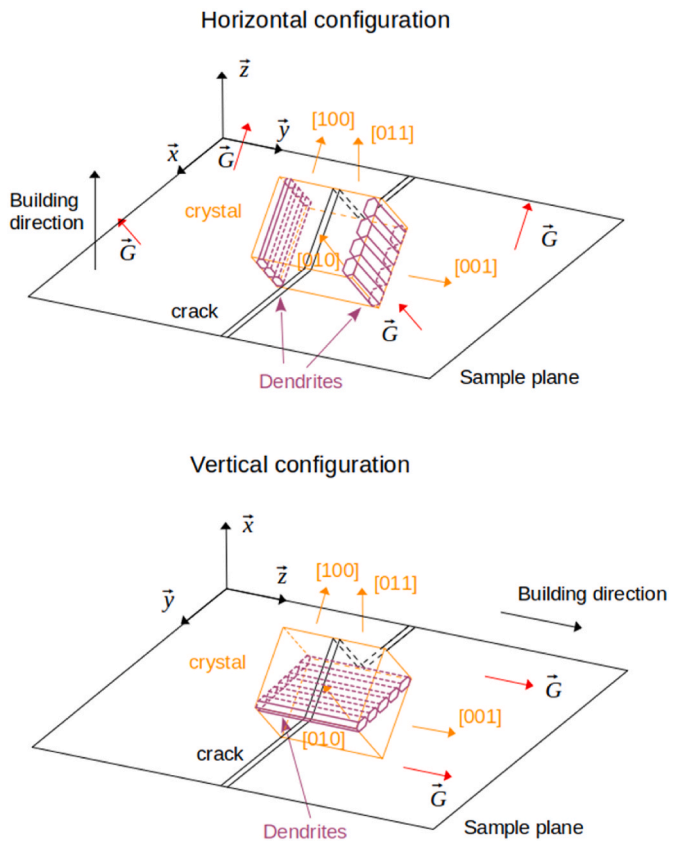

Fig. 8. – Illustration of the dominant crystal orientation beneath the crack in the microsized samples for horizontal and vertical manufacturing conditions.

from a sample to another is reduced for the vertical configuration compared to the horizontal one as observed experimentally. On the other hand, the dendrite axis, inherited from the thermal gradients during the process, with respect to the crack plane, is totally different between the two building configurations. In the horizontal configuration, as represented on Fig. 8, dendrite walls are parallel to the crack plane whereas a perpendicular relationship is observed for the vertical configuration. Considering the average size of the primary dendrite arm spacing of about 0.4 µm for this material with similar manufacturing conditions [23], the crack is likely to propagate inside a dendrite wall area characterized by a very high dislocation density in the horizontal configuration. In the vertical case, such crack to dendrite walls interaction is not possible, which may explain the difference in average fracture toughness for the two configurations. The reason of the improved fracture toughness for the horizontal configuration may be either related to that feature or to the presence of multiple grains which are more likely to occur compared to the vertical one.

Those features highlight the different fracture mechanisms involved at each scale. At the macro-polycrystalline level, fracture toughness is controlled by the interactions of the crack with the grain boundaries having different dominant orientations depending on the manufacturing conditions, mainly aligned with the crack plane for the horizontal configuration and perpendicular to this plane for the vertical one [21]. This polycrystalline configuration is detrimental to the crack initiation and propagation as more energy is required due to the different grain to grain plastic interactions as well as the crack path deviation due to grain boundaries. Consequently, as already reported previously by the authors, for macro specimens, fracture exhibit generally both intragranular and intergranular character [21,23]. At the micro-single crystalline level, such energy dissipation is restricted due to the single or multiple crystal character (few grains at maximum) leading to much lower fracture toughness values which seems to depends, at this scale, on the dendrite orientation with respect to the crack plane as well as on the probability to have a crack to grain boundary interaction. In that case, fracture is, obviously, fully intragranular.

When it comes to the intragranular fracture mechanisms, at the macro scale, it is driven by (i) the crack tip blunting caused by local plastic deformation near the crack tip – (ii) the pore formation/growth/coalescence followed by the extension of these pores under mechanical loading and finally the merging of the pores with the blunted crack. In the case of Hastelloy X manufactured by LPBF considered here, the pore formation is associated with the material debonding around nano inclusions of about 50 nm, generally located inside the interdendritic space [21,23] or larger scale precipitate with either intra or intergranular location [21,23]. Sample porosity plays a secondary role as the LPBF samples are almost fully dense in the manufacturing condition [23].

At the micro scale, similar intragranular mechanisms are expected. Fig. 9 illustrates the fractured surface for a micro specimen for the vertical configuration. Despite the low magnification, no micrometric voids are observed suggesting that ductile fracture occur on due to the matrix decohesion on the interdendritic nano inclusions (nanometric voids). Due to the reduced dimensions of those samples, grain boundaries, large sized inclusions or even pores (arising from entrapped gas during manufacturing) are unlikely to appear beneath the crack tip. Intragranular fracture mechanisms seems, hence, not to be affected by the testing scale.

3.4. *Application of a simple size-effect analytical model*

Once the fracture energy is quantified for all the tests configurations, the approach developed by Bazant et al. (see section 2.2.4) has been applied to the database to determine its relevance to account for size-effects in LPBF-HX specimens depending on their building direction (Fig. 10). As was pointed out in section 3.2, when the sample size is smaller than the Irwin plastic zone, the fracture behavior significantly changes, and there is an inherent length scale that governs the fracture behavior (hence the fracture toughness values). Based on equations (8) and (9)-10), the parameters of the size effect model have been identified for both testing configurations (Table 5).

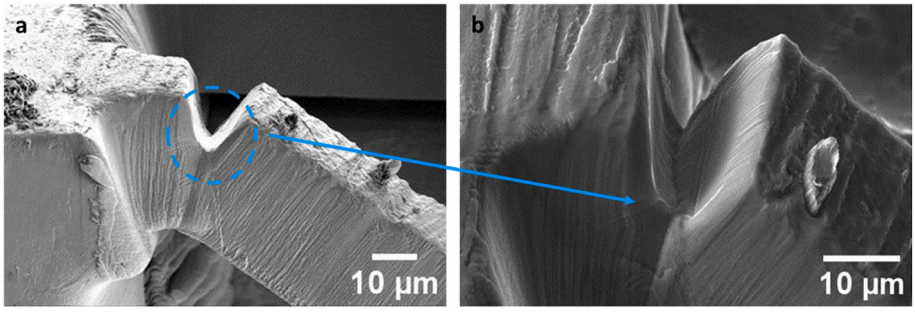

Fig. 9. – SEM observations of the ductile tearing of micro-cantilever HX specimens (Vertical configurations).

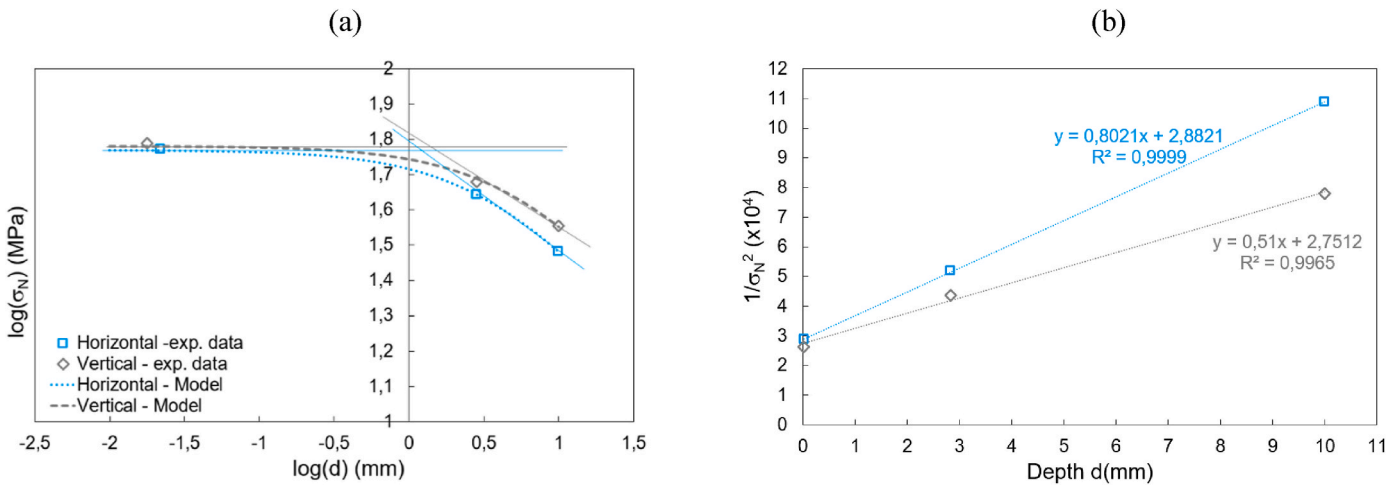

Fig. 10. – Bazant model application to both testing configurations (horizontally and vertically built specimens): (a) Size effect law – (b) Regression analysis.

Table 5
– Parameters of the size effect law (equations (9) and (10)) for both testing configurations.

	A	C	d_0 (mm)	m	n	k_0	k_1
Horizontal	$8.02.10^{-5}$	$2.88.10^{-4}$	1.33	0.2	4	3535	3
Vertical	$5.10.10^{-5}$	$2.75.10^{-4}$	1.57	0.2	4	1605	38

This model provides the inherent length scale d_0, which is a key parameter, associated with the transition from small to large scale. In horizontal specimens, the value of d_0 is about 1.33 mm, whereas it slightly increases to $d_0 = 1.57mm$ in vertical specimens (Fig. 10). This size effect model provides a simple design law to determine the R-curves of Hastelloy X micro-cantilevers printed by LPBF (LPBF-HX) in horizontal and vertical test configurations (Fig. 11). Finally, the model is particularly well adapted for describing the trends observed experimentally, but further analyses on an intermediate scale would be relevant to confirm its representativeness at different scales.

The knowledge of the internal characteristic length is important for LPBF metals because it governs the nonlocal softening behavior and fracture process. The d_0 value defines the zone over which stress or strain localizes in H and V specimens before fracture, and it represents the size of the FPZ, helping to transition from distributed plasticity to localized fracture. Finally, the ratio of the internal characteristic length to the structure size determines whether the failure is ductile (plastic deformation-dominated) or brittle (crack-dominated). This is crucial for designing LPBF parts in applications such as aerospace and nuclear industries, where metal failure prediction is critical.

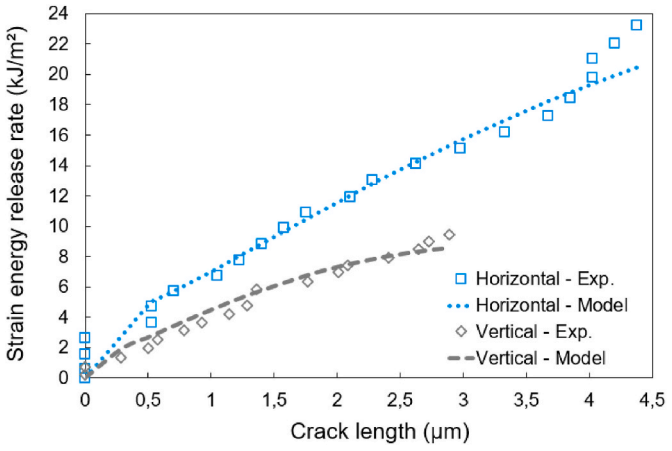

Fig. 11. – Comparison of simulated and experimental R-curves of Hastelloy X micro-cantilevers printed by LPBF in horizontal and vertical test configurations.

In the present work, the quantification of RS and their role on fracture mechanisms was not addressed as would require a full study by itself. As was shown by Bastola et al., the RS are expected to be higher in the V configuration, what could be either beneficial or detrimental to cracking [35].

4. Conclusions

This works aimed at investigating the influence of the microstructure anisotropy and size effects on the ductile failure of Hastelloy X elaborated by Laser Power Bed Fusion (LPBF-HX) by means of bending tests on notched cantilevers. The following conclusions are.

- The mechanical response and the fracture behavior of LPBF-HX micro-cantilever specimens (a few tens of μm) are characterized by a ductile tearing rather than a conventional crack propagation.
- In-situ SEM tests allow the crack growth to be monitored during mechanical loading, which is a key factor to estimate the fracture toughness values.
- The application of the data reduction method inspired from the application of the ASTM E1820 fracture testing standard provides the R-curves at the microscopic scale.
- The initial notch orientation with respect to lasing planes plays a significant role on the value of the fracture toughness at initiation but also in the fracture energy required to propagate the crack.
- The "composite" microstructure of LPBF-HX specimens consisting of layers (about 40 μm-thick layers) and its anisotropy characterized by different grain sizes and morphologies (equiaxed and elongated grains) are instrumental in ruling the crack initiation and propagation within micro-cantilevers.
- The application of Bazant's size-effect model allows the inherent length scale d_0 to be identified in both building configurations. It represents the size of the Fracture Process Zone, helping to transition from distributed plasticity to localized fracture.

Additional fracture testing at intermediate scale (a few hundreds of μm) would be relevant to further validate the applicability of the size-effect model. Also, tests with different cantilever geometries (e.g., varying thickness or notch depth) should be conducted to assess the robustness of parameter B of Bazant's model to generalize its applicability.

Declaration of competing interest

On behalf of my co-authors, I confirm that there is no conflict of interest regarding the publication of the present work untitled "*Synergy between microstructure anisotropy and size effects on the ductile failure of Hastelloy X printed by Laser Power Bed Fusion*".

Data availability

Data will be made available on request.

References

[1] S.S. Joshi, C. Keller, E. Hug, W. Lefebvre, Quantifying microstructural contribution to yield stress and strain hardening of Ni20Cr alloy manufactured by laser powder bed fusion with different volumetric energy densities, J. Alloys Compd. 968 (2023) 172241.

[2] S.S. Joshi, C. Keller, L. Mas, W. Lefebvre, E. Hug, J.P. Couzinie, On the origin of the strain hardening mechanisms of Ni20Cr alloy manufactured by laser powder bed fusion, Int. J. Plast. 165 (2023) 103610.

[3] P.N. Parent, J. Paris, J. Alexis, C. Boher, Influence of the scanning strategy on the microstructure and the tribological behavior of a Ni-based superalloy processed by
L-PBF additive manufacturing, Wear 564 (2025) 205671.

[4] N.A. Fleck, G.M. Muller, M.F. Ashby, J.W. Hutchinson, Strain gradient plasticity: theory and experiment, Acta Metall. Mater. 42 (2) (1994) 475–487.

[5] S. Shim, H. Bei, M.K. Miller, G.M. Phar, E.P. George, Effects of focused ion beam milling on the compressive behavior of directionally solidified micropillars and the nanoindentation response of an electropolished surface, Acta Mater. 57 (2009) 503–515.

[6] R. Pippan, S. Wurster, D. Kiener, Fracture mechanics of micro samples: fundamental considerations, Mater. Des. 159 (2018) 252–267.

[7] A. Muñoz-Ibáñez, J. Delgado-Martín, R. Juncosa-Rivera, Size effect and other effects on mode I fracture toughness using two testing methods, Int. J. Rock Mech. Min. Sci. 143 (2021) 104785.

[8] M.R. Ayatollahi, J. Akbardoost, Size effects on fracture toughness of quasi-brittle materials – a new approach, Eng. Fract. Mech. 92 (2012) 89–100.

[9] M. Alfreider, D. Kozic, O. Kolednik, D. Kiener, In-situ elastic-plastic fracture mechanics on the microscale by means of continuous dynamical testing, Mater. Des. 148 (2018) 177–187.

[10] M. Srinivas, G. Malakondaiah, R.W. Armstrong, P. Rama Rao, Ductile fracture toughness of polycrystalline armco iron of varying grain size, Acta Metall. Mater. 39 (5) (1991) 807–816.

[11] Z.P. Bažant, J.-K. Kim, P.A. Pfeiffer, Nonlinear fracture properties from size effect tests, J. Struct. Eng. 112 (2) (1986) 289–307.

[12] Z.P. Bažant, R. Gettu, M.T. Kazemi, Identification of nonlinear fracture properties from size effect tests and structural analysis based on geometry-dependent R-curves, Int. J. Rock Mech. Min. Sci. Geomech. Abstracts 28 (1) (1991) 43–51.

[13] S. Brinckmann, C. Kirchlechner, G. Dehm, Stress intensity factor dependence on anisotropy and geometry during micro-fracture experiments, Scr. Mater. 127 (2017) 76–78.

[14] Z.X. Wang, J.S. Hui, L. Jian, Experimental evaluation of the size effect on the ductile and brittle fracture toughness of a steel pressure vessel. Materials Science Forum, Trans Tech Publications, Ltd., 2009.

[15] H. Qiu, T. Hanamura, S. Torizuka, Influence of grain size on the ductile fracture toughness of ferritic steel, ISIJ Int. 54 (8) (2014) 1958–1964.

[16] S. Wurster, C. Motz, R. Pippan, Characterization of the fracture toughness of micro-sized tungsten single crystal notched specimens, Philos. Mag. 92 (14) (2012) 1803–1825.

[17] J. Ast, T. Przybilla, V. Maier, K. Durst, M. Göken, Microcantilever bending experiments in NiAl - Evaluation, size effects, and crack tip plasticity, J. Mater. Res. 29 (18) (2014) 2129–2140.

[18] P. Gruenewald, F. Schaefer, M. Thielen, M. Marx, C. Motz, Small-scale fracture mechanics of ductile materials: advantage of fatigue precracks and comparison of J-integral evaluations, Materialia 4 (2018) 104–108.

[19] J. Ast, M. Ghidelli, K. Durst, M. Göken, M. Sebastiani, A.M. Korsunsky, A review of experimental approaches to fracture toughness evaluation at the micro-scale, Mater. Des. 173 (2019) 107762.

[20] R. Huang, Y. Sun, C. Tan, D. Lin, X. Song, H. Zhao, Investigation of microstructure and failure mechanisms at room and elevated temperature of hastelloy X produced by laser powder-bed fusion, Next Mater. 2 (2024) 100142.

[21] B. Vieille, A. Duchaussoy, S. Benmabrouk, R. Henry, C. Keller, Fracture behavior of hastelloy X elaborated by laser powder bed fusion: influence of microstructure and building direction, J. Alloys Compd. 918 (2022) 165570.

[22] M.J. Paul, J.J. Kruzic, U. Ramamurty, B. Gludovatz, The importance of fracture toughness evaluation for additively manufactured metals, Acta Mater. 276 (2024) 120061.

[23] C. Keller, M. Mokhtari, B. Vieille, H. Briatta, P. Bernard, Influence of a rescanning strategy with different laser powers on the microstructure and mechanical properties of hastelloy X elaborated by powder bed fusion, Materials Science and Engineering: A 803 (2021) 140474.

[24] D. Kiener, C. Motz, M. Rester, M. Jenko, G. Dehm, FIB damage of Cu and possible consequences for miniaturized mechanical tests, Mater. Sci. Eng. 459 (1–2) (2007) 262–272.

[25] ASTM E1820-01, Standard Test Method for Measurement of Fracture Toughness, ASTM International, West Conshohocken, PA, 2001.

[26] G.C. Sih, E.P. Chen, Cracks in composite materials, in: G.C. Sih (Ed.), Mechanics of Fracture, 6, Martinus Nijoff Publishers, London, 1981.

[27] H. Tada, P.C. Paris, G.R. Irwin, The Stress Analysis of Cracks Handbook, ASME Press. Third Edition, January 2000.

[28] O. El Khatib, G. Hütter, R.D. Pham, A non-iterative parameter identification procedure for the non-local Gurson–Tvergaard–Needleman model based on standardized experiments, Int. J. Fract. 241 (2023) 73–94.

[29] Z.P. Bažant, Size effect in blunt fracture: concrete, rock, metal, J. Eng. Mech. 110 (4) (1984) 518–535.

[30] Z.P. Bažant, M.T. Kazemi, Determination of fracture energy, process zone length and brittleness number from size effect, with application to rock and concrete, Int. J. Fract. 44 (1990) 111–131.

[31] J.R. Rice, Elastic-Plastic fracture mechanics, in: Mechanics of Fracture, Symposium at ASME Winter Annual Meeting, 19, ASCE AMD, New York, 1976, pp. 23–53.

[32] M. Gattu, S. Aala, Size-effect method to determine mode-I fracture toughness of aluminium alloys, Eng. Fract. Mech. 242 (2021) 107504.

[33] H.T. Nguyen, A.A. Dönmez, Z.P. Bažant, Structural strength scaling law for fracture of plastic-hardening metals and testing of fracture properties, Extreme Mechanics Letters 43 (2021) 101141.

[34] D.A. Ferreira, R. Savioli, D.F.B. Sarzosa, New formulation for fracture toughness characterization using four-point bend specimens, Eng. Fract. Mech. 241 (2020) 107409.

[35] N. Bastola, M.P. Jahan, N. Rangasamy, C.S. Rakurty, A review of the residual stress generation in metal additive manufacturing: analysis of cause, measurement, effects, and prevention, Micromachines 14 (7) (2023) 1480.

[36] K. Krompholz, E.D. Grosser, K. Ewert, Determination of J-integral R-curves for Hastelloyx X and Inconel 617 up to 1223K using the potential drop technique, Mater. Werkst. 13 (1982) 236–244.